SHORT REPORT

A novel missense mutation in *CCDC88C* activates the JNK pathway and causes a dominant form of spinocerebellar ataxia

Ho Tsoi,[1,2] Allen C S Yu,[2] Zhefan S Chen,[1,2] Nelson K N Ng,[1,2] Anne Y Y Chan,[3] Liz Y P Yuen,[4] Jill M Abrigo,[5] Suk Ying Tsang,[2,6] Stephen K W Tsui,[7] Tony M F Tong,[8] Ivan F M Lo,[8] Stephen T S Lam,[8] Vincent C T Mok,[3] Lawrence K S Wong,[3] Jacky C K Ngo,[2] Kwok-Fai Lau,[2] Ting-Fung Chan,[2,6] H Y Edwin Chan[1,2]

▸ Additional material is published online only. To view please visit the journal online (http://dx.doi.org/10.1136/jmedgenet-2014-102333).

For numbered affiliations see end of article.

Correspondence to
Dr H Y Edwin Chan, School of Life Sciences, Room 509B, Mong Man Wai Building, The Chinese University of Hong Kong, Hong Kong, Hong Kong; hyechan@cuhk.edu.hk
Dr Ting-Fung Chan, School of Life Sciences, Room 177, Science Centre South Block, The Chinese University of Hong Kong, Hong Kong; tf.chan@cuhk.edu.hk

HT and ACSY contributed equally.

Received 10 February 2014
Revised 9 June 2014
Accepted 5 July 2014
Published Online First 25 July 2014

To cite: Tsoi H, Yu ACS, Chen ZS, *et al*. *J Med Genet* 2014;**51**:590–595.

ABSTRACT

Background Spinocerebellar ataxias (SCAs) are a group of clinically and genetically diverse and autosomal-dominant disorders characterised by neurological deficits in the cerebellum. At present, there is no cure for SCAs. Of the different distinct subtypes of autosomal-dominant SCAs identified to date, causative genes for only a fraction of them are currently known. In this study, we investigated the cause of an autosomal-dominant SCA phenotype in a family that exhibits cerebellar ataxia and pontocerebellar atrophy along with a global reduction in brain volume.

Methods and results Whole-exome analysis revealed a missense mutation c.G1391A (p.R464H) in the coding region of the *coiled-coil domain containing 88C* (*CCDC88C*) gene in all affected individuals. Functional studies showed that the mutant form of CCDC88C activates the c-Jun N-terminal kinase (JNK) pathway, induces caspase 3 cleavage and triggers apoptosis.

Conclusions This study expands our understanding of the cause of autosomal-dominant SCAs, a group of heterogeneous congenital neurological conditions in humans, and unveils a link between the JNK stress pathway and cerebellar atrophy.

We identified a spinocerebellar ataxia (SCA) family in Hong Kong, China (figure 1A). The proband (II:4) is a 65-year-old woman with disease onset at 43 years of age and was presented with insidious onset of unsteady gait and dysarthria. After 10 years of disease onset, she required to walk with a cane. After 18 years of disease onset, she became wheelchair user due to severe ataxia. Neurological examination showed ocular dysmetria, scanning speech, intentional tremor, dysdiadokokinesia, brisk reflexes (3+) with ankle clonus and wide-based gait. Her latest Scale for the Assessment and Rating of Ataxia (SARA) score was 24/40 (table 1). MRI of the proband's brain showed pontocerebellar atrophy and normal corpus callosum (figure 1B; table 2). Individual II:5 (a younger brother of the proband) is a 62-year-old male with disease onset at 42 years of age and was presented with ataxic gait and dysarthria. After 10 years of disease onset, he required to walk with a cane; and after 17 years of disease onset, he became wheelchair user. Neurological examination showed ocular dysmetria, impaired vertical gaze, scanning speech, ataxic gait and spastic paraparesis. His latest SARA score was 22/40 (table 1), and MRI of the brain showed moderate pontocerebellar atrophy (table 2). Both patients had no history of alcohol abuse, parkinsonism features nor peripheral neuropathy.

The proband was screened negative for SCAs 1, 2, 3, 6, 7, 8 and 12. Six individuals of this family, including four affected and two unaffected (figure 1A), were recruited for a whole-exome sequencing analysis. Sequencing libraries were prepared using standard Illumina paired-end DNA preparation protocols, followed by exome enrichment using the Illumina TruSeq Exome Enrichment method. Paired-end sequencing was performed on an Illumina HiSeq2000 system, generating 100 bp paired-end reads with an average coverage of 102× in the targeted exonic regions (62 Mb) (see online supplementary table S1). The filtered exome sequencing reads were mapped to the human genome (GRCh37/hg19) with Novoalign 2.08 (Novocraft Technologies Sdn Bhd, Malaysia), followed by alignment postprocessing steps including PCR duplicates removal, sample-level indels realignment and base quality recalibration using Picard and Genome Analysis Toolkit (GATK) 2.5.[1] A union set of 328 328 raw variants was identified among all samples using GATK UnifiedGenotyper 2.5 (see online supplementary table S2). Snpeff[2] was used to annotate the predicted functional consequences of the variants. The raw variants were filtered according to the V.4 of GATK best practice for variant detection,[3] while variants outside of the targeted enrichment regions were removed (see online supplementary methods). Recent developments in bioinformatics algorithms allow reliable genotyping of short tandem repeats (STRs) using high-throughput sequencing data.[4–8] We have analysed STRs variations in the coding, intronic and untranslated regions of genes known to be associated with SCA using LobSTR[7] and RepeatSeq,[8] and none of the identified STR variation matched with the observed co-segregation pattern.

Coupling exome sequencing with family-based genetic linkage analysis can largely reduce the search space for loci that are putatively responsible for Mendelian diseases.[9] By adopting such strategy, 7 443 filtered heterozygous single nucleotide

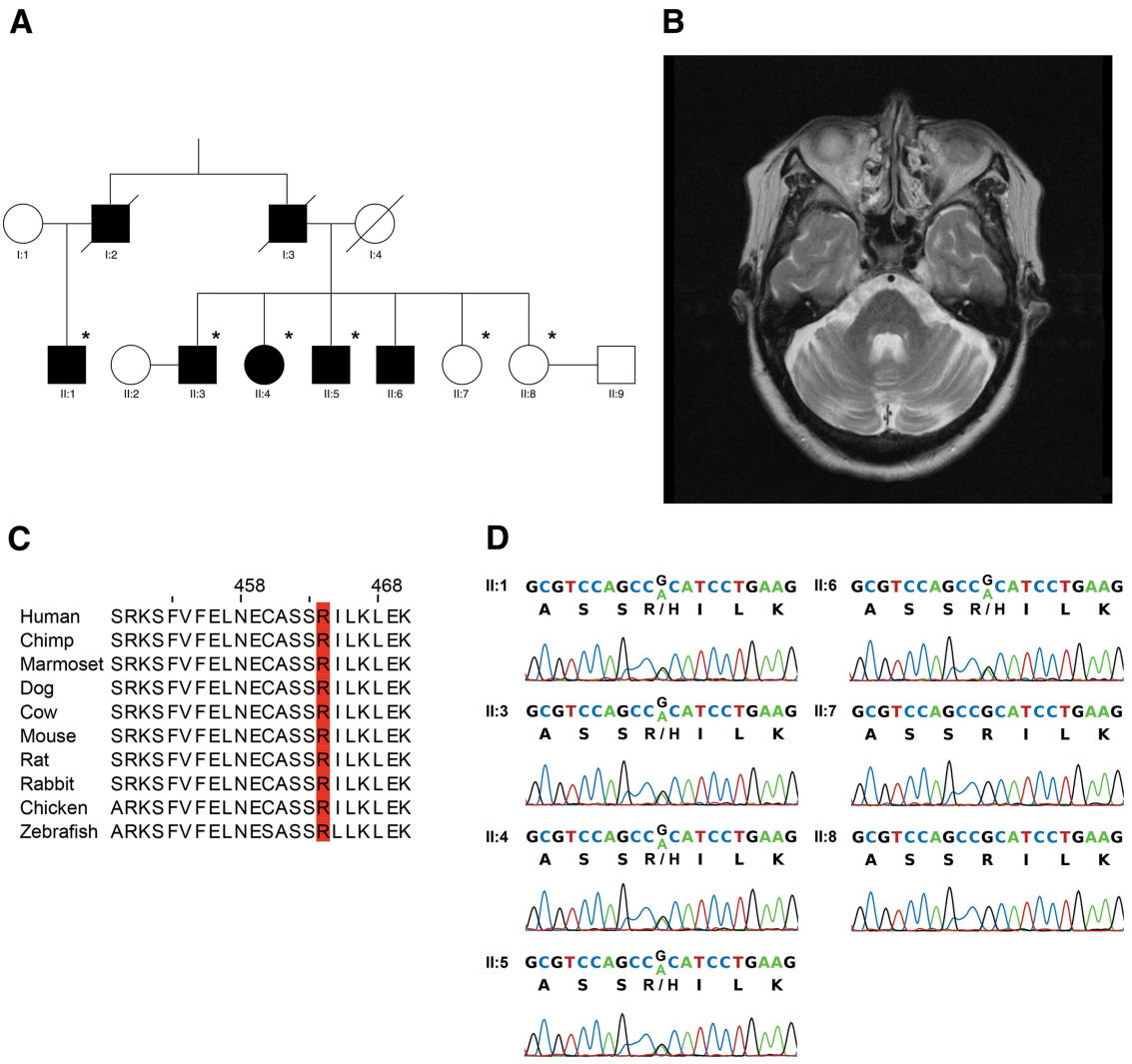

Figure 1 A family with an autosomal-dominant missense p.R464H mutation in coiled-coil domain containing 88C (CCDC88C) at a location with high conservation. (A) The pedigree under study. Six members of the family, which are marked with asterisk, were recruited for whole-exome sequencing analysis. (B) Axial T2-weighted MRI of the brain of proband (II:4) showed mild atrophy of the pons and cerebellar hemispheres. (C) The arginine^{464} location in CCDC88C is highly conserved among different vertebrate species. (D) The c.G1391A mutation in *CCDC88C* was validated by Sanger sequencing, which revealed perfect segregation with the ataxia of the pedigree.

polymorphism (SNP) markers with an average heterozygosity of 0.45 were selected for genetic linkage analysis. Finally, MERLIN[10] was used for multipoint parametric linkage analysis, where a rare dominant disease model with disease allele frequency of 0.00001 was specified. Four peak regions with log of odds (LOD) scores >2 were identified on chromosomes 11, 14, 18 and 20 (see online supplementary figure S1 and methods). Upon annotation of the variants in these four LOD peak regions, it was found that none of the variants in promoter, UTR, microRNA or other non-coding RNA regions fit the observed autosomal-dominant inheritance pattern. Accordingly, synonymous mutations and non-coding mutations were discarded, leaving 13 mutations in the coding region that matched the observed inheritance pattern. Variant calling of these four LOD peak regions on chromosomes 11, 14, 18 and 20 was repeated using GATK haplotypecaller V.2.5 and FreeBayes V.0.9.9,[11] both returning an identical list of the 13 candidate variants after the aforementioned filtering steps.

To further exclude common variants, which are unlikely to be causative, we excluded variants with a minor allele frequency greater than 0.005 and not reported as pathogenic according to online databases, including dbSNP (V.138),[12] 1000 Genomes Project (phase I release V.3),[13] HapMap release 28[14] and NHLBI Exome Sequencing Project (ESP6500SI-V2).[15] Only three heterozygous candidate variants remained after this filtering step (see online supplementary tables S3 and S4). We next assessed the gene expression profile of the candidates using NCBI UniGene build 236 (UniGene)[16] EST profile and found that the *coiled-coil domain containing 88C* (*CCDC88C*) gene,[17 18] also known as *Dvl-associating protein with a high frequency of leucine residues* (*DAPLE*),[19] is the only candidate that expresses in brain (see online supplementary table S4). Gene expression data from Allen Brain Atlas[20] and Human Brain Transcriptome Project[21] also showed that *CCDC88C* has the highest average expression level in cerebellum (see online supplementary table S4). Next, the pathogenicity of the three remaining candidate mutations was evaluated using five functional predictors (see online supplementary methods). Only the NM_001080414:c.G1391A candidate mutation in *CCDC88C*, which causes a missense p.R464H mutation in the protein, was

Table 1 Clinical assessments of the affected members of the pedigree

	II:4	II:5
Gait (0–8)	7	7
Stance (0–6)	6	6
Sitting (0–4)	1	0
Speech disturbance (0–6)	3	2
Finger chase (R+L)/2 (0-4)	1	2
Nose-finger test (R+L)/2 (0-4)	1	0
Fast alternating hand movements (R+L)/2 (0–4)	3	3
Heel-shin slide (R+L)/2 (0–4)	2	2
Total SARA score (0–40)	24	22

To determine the severity of the patients, neurological examinations were performed based on the Scale for the Assessment and Rating of Ataxia (SARA). In brief, the SARA instrument consists of eight test components: (1) gait; (2) stance; (3) sitting; (4) speech disturbance; (5) finger chase; (6) nose-finger test; (7) fast alternating hand movement and (8) heel-shin slide. A good correlation between SARA results and spinocerebellar ataxia (SCA) disease stages has been validated in a large-scale study by EUROSCA. SARA is now widely accepted as a clinical assessment scale for SCAs and has also been used as a reliable measurement instrument for the severity of SCAs in the Asian population, including in China. The higher the SARA score, the more severe the ataxia symptoms the patient presents.

unanimously predicted to be disease-causing by all predictors (see online supplementary table S4). It is also of note that the arginine^{464} residue is situated in an evolutionarily conserved region of the protein, which further highlights the functional implication of the p.R464H variation in CCDC88C protein activity (figure 1C and online supplementary figure S5). We next Sanger sequenced all generation II individuals of this pedigree and found that the *CCDC88C* c.G1391A candidate mutation segregated perfectly with the SCA manifestation (figure 1A,D). To check whether c.G1391A could be a common variant among the local population, 199 local healthy subjects were screened by Sanger sequencing and none of these control subject harbours such variation. Taking into account all evidence presented above, we postulated that the *CCDC88C* c.G1391A variant is the most probable SCA-causing mutation for the family. Since *CCDC88C* had not been previously reported to be associated with SCA,[22] this locus was assigned as SCA40 by the HUGO Gene Nomenclature Committee (http://www.genenames.org/).

Table 2 A summary of neuroimaging findings of affected members of the pedigree

Patient	II:4	II:5
Age at imaging (years)	61	64
MRI sequence	Axial and sagittal T1 SE, T2 TSE Coronal FLAIR	Axial and sagittal T1 SE, T2 TSE Coronal FLAIR
Cerebrospinal fluid spaces	Prominent 4th ventricle and posterior fossa subarachnoid space	Prominent 4th ventricle and posterior fossa subarachnoid space
Vermis and cerebellar atrophy	Mild	Mild to moderate
Pons atrophy	Mild	Mild
Posterior cranial fossa size	Normal	Normal
Retrocerebellar cyst	None	None
White matter changes	Linear and punctate subcortical T2W hyperintensities (++)	Linear and punctate subcortical T2W hyperintensities (+)

FLAIR, fluid attenuated inversion recovery; TSE, turbo spin echo, SE, spin echo.

The c-Jun N-terminal kinase (JNK) pathway has been reported in cerebellar neuronal cell death,[23 24] and the hyperphosphorylation of JNK triggers apoptosis.[25] The role of JNK activation and c-Jun phosphorylation has also been described in the cerebellar granule cell death.[26 27] Further, alteration of JNK and caspase signalling cascades has been reported in different SCA conditions.[22] It was previously reported that when the mRNA that encodes the *Xenopus* CCDC88C orthologue, *Xenopus* Daple-like (XDal), was co-injected with *c-Jun* mRNA into two-cell *Xenopus* embryos, *XDal* was capable of inducing c-Jun phosphorylation.[28] All of the above observations prompted us to investigate the involvement of the JNK pathway in the pathogenesis of SCA40. We first examined the JNK phosphorylation status in primary fibroblasts isolated from a patient (II:5) and observed JNK hyperphosphorylation in the patient cells (figure 2A). When compared with II:5, JNK hyperphosphorylation was not detected in fibroblasts isolated from the unaffected sibling II:7 (figure 2A). Further, we showed that knockdown of *CCDC88C* expression in patient fibroblasts reduced JNK hyperphosphorylation (figure 2A). This clearly indicates an association between the CCDC88C p.R464H mutation and JNK hyperphosphorylation.

To further confirm the pathogenic effect of the CCDC88C p.R464H mutation, we overexpressed mutant (MT) CCDC88C protein in human HEK293 cells and determined whether it would modulate the JNK pathway. Our data showed that both wild type (WT) and MT CCDC88C proteins were capable of inducing JNK hyperphosphorylation, and the MT protein was found to be more prominent in promoting it compared with the wild type (WT) (see online supplementary figures S2 and S3). Further, the total JNK protein level in CCDC88C-expressing cells was comparable to the untransfected control. This clearly indicates that CCDC88C only modulates the phosphorylation status but not the cellular expression of JNK (see online supplementary figures S2 and S3). Taken together, our data are in line with a previous report that showed that the *Xenopus* orthologue of *CCDC88C*, *XDal*, plays a modulatory role in the JNK pathway[28] (see online supplementary figure S3). We also examined whether overexpression of the other two candidates, CHRDL2 and KCNK13 (see online supplementary table S4), would induce JNK hyperphosphorylation. In contrast to CCDC88C, neither CHRDL2 nor KCNK13 was found to promote phosphorylation of JNK (see online supplementary figure S2).

As the transfection of 0.2 μg of *CCDC88C p.R464H* mutant expression construct was already capable of inducing JNK hyperphosphorylation (see online supplementary figure S3), 0.5 μg of the mutant construct was thus used in our subsequent biochemical experiments with the aim to minimise any potential non-specific cellular effect (figure 2B and online supplementary figure S4A). In contrast to MT CCDC88C overexpression, knockdown of endogenous *CCDC88C* expression did not result in any alteration of JNK phosphorylation (figure 2B and online supplementary figure S4B). This argues that p.R464H confers a gain-of-function property to CCDC88C. Furthermore, we detected prominent c-Jun phosphorylation in HEK293 cells overexpressed with MT CCDC88C protein, and such effect was abolished when cells were treated with the JNK-specific inhibitor SP600125 (figure 2C). This indicates that the MT CCDC88C-mediated c-Jun phosphorylation is JNK dependent.

We next determined whether MT CCDC88C would induce apoptosis. Proteolytic cleavage of caspase 3 is a commonly used

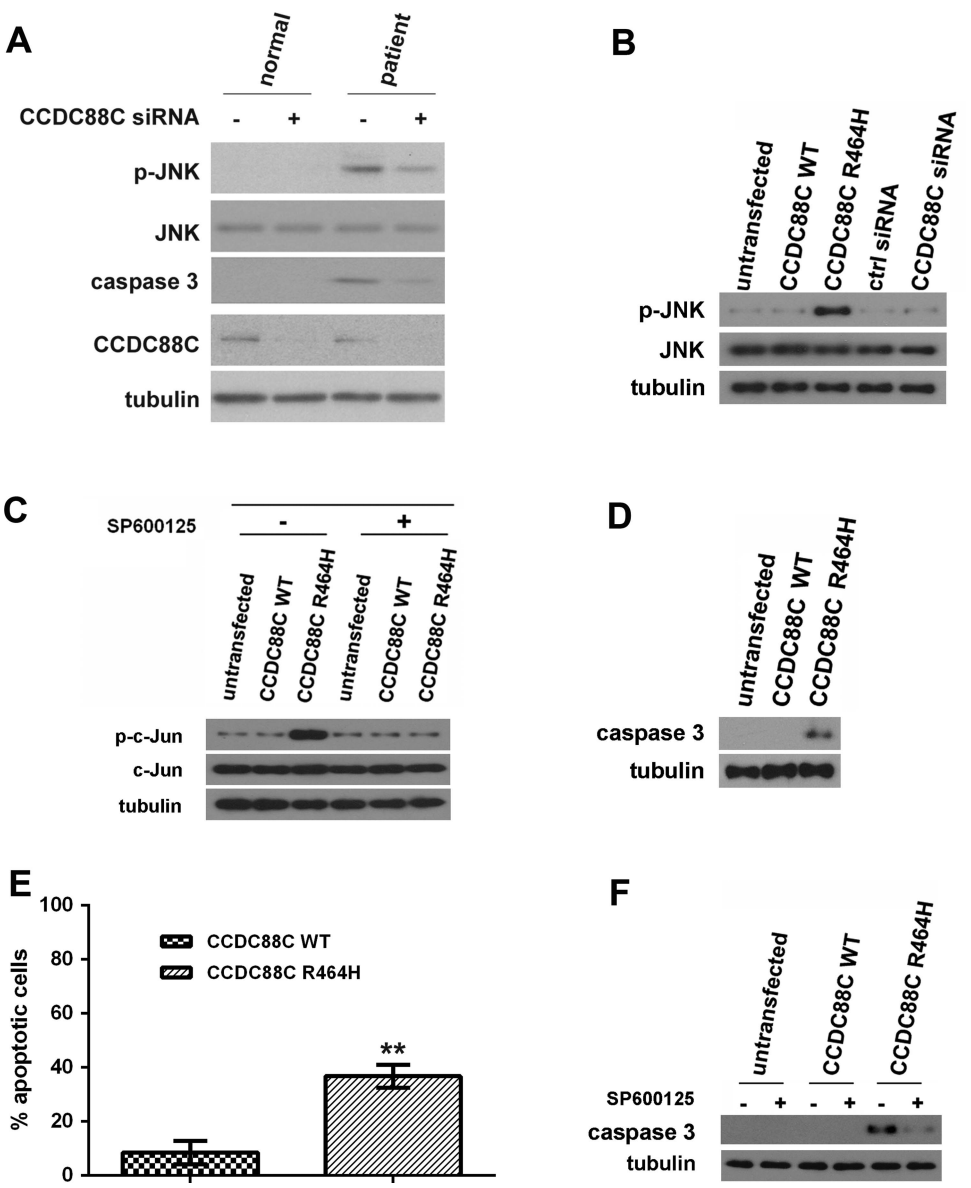

Figure 2 Coiled-coil domain containing 88C (CCDC88C) protein carrying the R464H mutation activated c-Jun N-terminal kinase (JNK) and caspase 3 apoptotic pathways. (A) Increased level of phosphorylated JNK was detected in patient primary fibroblasts (II:5) but not in that isolated from the unaffected sibling (II:7). Skin fibroblasts were isolated and cultured as described.[31] Fibroblasts were treated with 5 pmol of ON-TARGETplus (Dharmacon) *CCDC88C* siRNA L-033364-00-0005 (+) or control (ctrl) siRNA (–). Total and phospho-JNK proteins were detected using anti-JNK 3708 (1:1 000, Cell Signaling Technology) and anti-p-JNK 5136 (1:1 000; Cell Signaling Technology) antibodies, respectively. Cleaved caspase 3 was detected by an antiactivated caspase 3 antibody Asp175 (1:5 00; Cell Signaling Technology). Endogenous CCDC88C was detected by anti-CCDC88C antibody A302-951A (1:1 000; Bethyl Laboratories). The experiment was repeated for at least three times. Only representative blots are shown. (B) Overexpression of mutant (MT) CCDC88C protein led to hyperphosphorylation of JNK in HEK293 cells. Both WT and MT *CCDC88C* expression constructs (0.5 μg) were used to transfect HEK293 cells. Cells were harvested 24 h after transfection. To knockdown *CCDC88C* expression, cells were treated with 5 pmol of ON-TARGETplus *CCDC88C* siRNA L-033364-00-0005 (Dharmacon) or control (ctrl) siRNA (Dharmacon). Cell lysates were analysed by western blotting with anti-JNK 3708 (1:1 000, Cell Signaling Technology) and anti-p-JNK 5136 (1:1 000; Cell Signaling Technology) antibodies. Neither the knockdown of *CCDC88C* WT expression nor its overexpression altered the level of JNK phosphorylation. The experiment was repeated for at least three times. Only representative blots are shown. (C) Phosphorylation of c-Jun was detected in HEK293 cells transiently expressing the CCDC88C MT protein. For JNK inhibitor treatment, cells were treated with 25 μM of SP600125 (Sigma) for 24 h. '+' and '−' denote cells with and without SP600125 treatment, respectively. Cell lysates were analysed by western blotting with anti-c-Jun 2315 (1:1 000, Cell Signaling Technology) and anti-p-c-Jun 9164 (1:1 000; Cell Signaling Technology) antibodies. The experiment was repeated for at least three times. Only representative blots are shown. (D) Overexpression of MT CCDC88C protein-induced caspase 3 activation in HEK293 cells. Cell lysates were analysed by western blotting and detected using an antiactivated caspase 3 antibody Asp175 (1:500; Cell Signaling Technology). The experiment was repeated for at least three times. Only representative blots are shown. (E) Overexpression of MT CCDC88C protein-induced apoptosis in HEK293 cells. Apoptosis was detected using the APO-BrdU TUNEL Assay Kit, with Alexa Fluor 488 Anti-BrdU (Life Technologies). The data represent means ±SD from four independent experiments. At least 100 cells were counted in each experiment. **denotes $p<0.005$. (F) Caspase 3 activation induced by MT CCDC88C protein expression can be blocked by JNK inhibitor. '+' and '−' denote cells with and without SP600125 treatment, respectively. The experiment was repeated for at least three times. Only representative blots are shown. Tubulin was used as loading control in all experiments and was detected using anti-β tubulin antibody E7 (1:10 000; Developmental Studies Hybridoma Bank).

readout for apoptotic cell death, and we detected caspase 3 cleavage in patient primary fibroblasts, and caspase 3 activation was reduced when *CCDC88C* expression was knocked down (figure 2A). Similar to the patient primary fibroblasts, we also detected apoptotic events in HEK293 cells overexpressing MT CCDC88C protein using caspase 3 cleavage (figure 2D) and TUNEL (figure 2E) assays. To investigate whether the caspase 3 activation we observed in MT CCDC88C-expressing cells (figure 2D) is mediated through the JNK pathway, we treated cells overexpressing the MT protein with the JNK-specific inhibitor SP600125. As expected, caspase 3 activation was reduced in SP600125-treated cells (figure 2F). Taken together, our results demonstrate that the JNK pathway is one mechanism that the MT CCDC88C protein exploits to induce apoptosis in SCA40.

The p.R464H mutation is located within a predicted HOOK domain (a.a. 9-597; Pfam: PF05622[29]) of CCDC88C (see online supplementary figure S5). In general, the HOOK family proteins function as adaptors to mediate various cellular functions, including protein trafficking and cilium formation.[30] We performed confocal microscopy to determine whether the p.R464H mutation would alter subcellular distribution of the MT CCDC88C protein. The WT protein was found to localise to the cytosol and around the perinuclear region (see online supplementary figure S6). We did not observe any change of the subcellular localisation pattern of the MT CCDC88C protein compared with that of the WT (see online supplementary figure S6). Our data suggest that the CCDC88C dominant missense mutation might alter the cellular properties of the mutant protein, for instance the HOOK domain function, which consequently leads to activation of the JNK and apoptotic pathways. In summary, we used whole-exome sequencing to identify the missense mutation c.G1391A (p.R464H) in *CCDC88C* from a SCA family. Our functional study demonstrated that this missense mutation confers a gain-of-function property to the MT CCDC88C protein and provides experimental evidence that link the JNK and caspase-mediated apoptotic pathways to the pathogenesis of SCA40.

Author affiliations
[1]Faculty of Science, Laboratory of *Drosophila* Research, School of Life Sciences, The Chinese University of Hong Kong, Hong Kong, Hong Kong
[2]Faculty of Science, Biochemistry Programme, School of Life Sciences, The Chinese University of Hong Kong, Hong Kong, Hong Kong
[3]Faculty of Medicine, Division of Neurology, Department of Medicine and Therapeutics, The Chinese University of Hong Kong, Hong Kong, Hong Kong
[4]Faculty of Medicine, Department of Chemical Pathology, The Chinese University of Hong Kong, Hong Kong, Hong Kong
[5]Faculty of Medicine, Department of Imaging and Interventional Radiology, The Chinese University of Hong Kong, Hong Kong, Hong Kong
[6]Partner State Key Laboratory of Agrobiotechnology, The Chinese University of Hong Kong, Hong Kong
[7]Faculty of Medicine, School of Biomedical Sciences, The Chinese University of Hong Kong, Hong Kong, Hong Kong
[8]Clinical Genetic Service, Department of Health, The Government of Hong Kong, Hong Kong, Hong Kong

Acknowledgements This publication is dedicated to the patients and families who have contributed to this study. We thank Ms Roxanna Liu, Miss Haley Chan, Ms Franco Lai and Ms Anita Cheng for technical support, and Dr Sheng-Han Kuo for critical reading of the manuscript.

Contributors HYEC, ACSY, HT, S-YT, SKWT, JCKN and K-FL conceived and designed the experiments; HT, ACSY, ZSC and T-FC performed the experiments; HYEC, LYPY, HT, ACSY, NKNN, S-YT and T-FC analysed the data; HYEC, TH and ACSY wrote the paper; AYYC, LKSW, VCTM, JMA, TMFT, IFML and STSL undertook patient management, collection of samples and delineation of the phenotype.

Funding This work was supported by a CUHK Department of Biochemistry (Science) Collaborative Research grant, The Hong Kong College of Physicians, Research Grants Council (RGC) of Hong Kong (AoE/M-05/12) and the Hong Kong Spinocerebellar Ataxia Association. ACSY and TFC are supported by the Lo Kwee-Seong Biomedical Research Fund and the Lee Hysan Foundation. This study was approved by the Joint Chinese University of Hong Kong-New Territories East Cluster Clinical Research Ethics Committee (ref. nos.: CRE-2012.361 and CRE-2013.120), and informed consent was obtained from both the healthy and affected members of the family.

Competing interests None.

Patient consent Obtained.

Ethics approval Joint Chinese University of Hong Kong-New Territories East Cluster Clinical Research Ethics Committee.

Provenance and peer review Not commissioned; externally peer reviewed.

REFERENCES

1 McKenna A, Hanna M, Banks E, Sivachenko A, Cibulskis K, Kernytsky A, Garimella K, Altshuler D, Gabriel S, Daly M, DePristo MA. The Genome Analysis Toolkit: a MapReduce framework for analyzing next-generation DNA sequencing data. *Genome Res* 2010;20:1297–303.
2 Cingolani P, Platts A, Wang le L, Coon M, Nguyen T, Wang L, Land SJ, Lu X, Ruden DM. A program for annotating and predicting the effects of single nucleotide polymorphisms, SnpEff: SNPs in the genome of Drosophila melanogaster strain w1118; iso-2; iso-3. *Fly (Austin)* 2012;6:80–92.
3 DePristo MA, Banks E, Poplin R, Garimella KV, Maguire JR, Hartl C, Philippakis AA, del Angel G, Rivas MA, Hanna M, McKenna A, Fennell TJ, Kernytsky AM, Sivachenko AY, Cibulskis K, Gabriel SB, Altshuler D, Daly MJ. A framework for variation discovery and genotyping using next-generation DNA sequencing data. *Nat Genet* 2011;43:491–8.
4 Adey A, Burton JN, Kitzman JO, Hiatt JB, Lewis AP, Martin BK, Qiu R, Lee C, Shendure J. The haplotype-resolved genome and epigenome of the aneuploid HeLa cancer cell line. *Nature* 2013;500:207–11.
5 McIver LJ, Fondon JW III, Skinner MA, Garner HR. Evaluation of microsatellite variation in the 1000 Genomes Project pilot studies is indicative of the quality and utility of the raw data and alignments. *Genomics* 2011;97:193–9.
6 Fondon JW III, Martin A, Richards S, Gibbs RA, Mittelman D. Analysis of microsatellite variation in Drosophila melanogaster with population-scale genome sequencing. *PLoS ONE* 2012;7:e33036.
7 Gymrek M, Golan D, Rosset S, Erlich Y. lobSTR: a short tandem repeat profiler for personal genomes. *Genome Res* 2012;22:1154–62.
8 Highnam G, Franck C, Martin A, Stephens C, Puthige A, Mittelman D. Accurate human microsatellite genotypes from high-throughput resequencing data using informed error profiles. *Nucleic Acids Res* 2013;41:e32.
9 Smith KR, Bromhead CJ, Hildebrand MS, Shearer AE, Lockhart PJ, Najmabadi H, Leventer RJ, McGillivray G, Amor DJ, Smith RJ, Bahlo M. Reducing the exome search space for mendelian diseases using genetic linkage analysis of exome genotypes. *Genome Biol* 2011;12:R85.
10 Abecasis GR, Cherny SS, Cookson WO, Cardon LR. Merlin—rapid analysis of dense genetic maps using sparse gene flow trees. *Nat Genet* 2002;30:97–101.
11 Garrison E, Marth G. Haplotype-based variant detection from short-read sequencing. arXiv:12073907 2012.
12 Sherry ST, Ward MH, Kholodov M, Baker J, Phan L, Smigielski EM, Sirotkin K. dbSNP: the NCBI database of genetic variation. *Nucleic Acids Res* 2001;29:308–11.
13 Abecasis GR, Altshuler D, Auton A, Brooks LD, Durbin RM, Gibbs RA, Hurles ME, McVean GA; Genomes Project C. A map of human genome variation from population-scale sequencing. *Nature* 2010;467:1061–73.
14 International HapMap CAltshuler DM, Gibbs RA, Peltonen L, Altshuler DM, Gibbs RA, Peltonen L, Dermitzakis E, Schaffner SF, Yu F, Peltonen L, Dermitzakis E, Bonnen PE, Altshuler DM, Gibbs RA, de Bakker PI, Deloukas P, Gabriel SB, Gwilliam R, Hunt S, Inouye M, Jia X, Palotie A, Parkin M, Whittaker P, Yu F, Chang K, Hawes A, Lewis LR, Ren Y, Wheeler D, Gibbs RA, Muzny DM, Barnes C, Darvishi K, Hurles M, Korn JM, Kristiansson K, Lee C, McCarrol SA, Nemesh J, Dermitzakis E, Keinan A, Montgomery SB, Pollack S, Price AL, Soranzo N, Bonnen PE, Gibbs RA, Gonzaga-Jauregui C, Keinan A, Price AL, Yu F, Anttila V, Brodeur W, Daly MJ, Leslie S, McVean G, Moutsianas L, Nguyen H, Schaffner SF, Zhang Q, Ghori MJ, McGinnis R, McLaren W, Pollack S, Price AL, Schaffner SF, Takeuchi F, Grossman SR, Shlyakhter I, Hostetter EB, Sabeti PC, Adebamowo CA, Foster MW, Gordon DR, Licinio J, Manca MC, Marshall PA, Matsuda I, Ngare D, Wang VO, Reddy D, Rotimi CN, Royal CD, Sharp RR, Zeng C, Brooks LD, McEwen JE. Integrating common and rare genetic variation in diverse human populations. *Nature* 2010;467:52–8.

15 Tennessen JA, Bigham AW, O'Connor TD, Fu W, Kenny EE, Gravel S, McGee S, Do R, Liu X, Jun G, Kang HM, Jordan D, Leal SM, Gabriel S, Rieder MJ, Abecasis G, Altshuler D, Nickerson DA, Boerwinkle E, Sunyaev S, Bustamante CD, Bamshad MJ, Akey JM, Broad GO, Seattle GO, Project NES. Evolution and functional impact of rare coding variation from deep sequencing of human exomes. *Science* 2012;337:64–9.
16 Wheeler DL, Church DM, Federhen S, Lash AE, Madden TL, Pontius JU, Schuler GD, Schriml LM, Sequeira E, Tatusova TA, Wagner L. Database resources of the National Center for Biotechnology. *Nucleic Acids Res* 2003;31:28–33.
17 Ekici AB, Hilfinger D, Jatzwauk M, Thiel CT, Wenzel D, Lorenz I, Boltshauser E, Goecke TW, Staatz G, Morris-Rosendahl DJ, Sticht H, Hehr U, Reis A, Rauch A. Disturbed Wnt signalling due to a mutation in CCDC88C causes an autosomal recessive non-syndromic hydrocephalus with medial diverticulum. *Mol Syndromol* 2010;1:99–112.
18 Drielsma A, Jalas C, Simonis N, Desir J, Simanovsky N, Pirson I, Elpeleg O, Abramowicz M, Edvardson S. Two novel CCDC88C mutations confirm the role of DAPLE in autosomal recessive congenital hydrocephalus. *J Med Genet* 2012;49:708–12.
19 Oshita A, Kishida S, Kobayashi H, Michiue T, Asahara T, Asashima M, Kikuchi A. Identification and characterization of a novel Dvl-binding protein that suppresses Wnt signalling pathway. *Genes Cells* 2003;8:1005–17.
20 Hawrylycz MJ, Lein ES, Guillozet-Bongaarts AL, Shen EH, Ng L, Miller JA, van de Lagemaat LN, Smith KA, Ebbert A, Riley ZL, Abajian C, Beckmann CF, Bernard A, Bertagnolli D, Boe AF, Cartagena PM, Chakravarty MM, Chapin M, Chong J, Dalley RA, Daly BD, Dang C, Datta S, Dee N, Dolbeare TA, Faber V, Feng D, Fowler DR, Goldy J, Gregor BW, Haradon Z, Haynor DR, Hohmann JG, Horvath S, Howard RE, Jeromin A, Jochim JM, Kinnunen M, Lau C, Lazarz ET, Lee C, Lemon TA, Li L, Li Y, Morris JA, Overly CC, Parker PD, Parry SE, Reding M, Royall JJ, Schulkin J, Sequeira PA, Slaughterbeck CR, Smith SC, Sodt AJ, Sunkin SM, Swanson BE, Vawter MP, Williams D, Wohnoutka P, Zielke HR, Geschwind DH, Hof PR, Smith SM, Koch C, Grant SG, Jones AR. An anatomically comprehensive atlas of the adult human brain transcriptome. *Nature* 2012;489:391–9.
21 Kang HJ, Kawasawa YI, Cheng F, Zhu Y, Xu X, Li M, Sousa AM, Pletikos M, Meyer KA, Sedmak G, Guennel T, Shin Y, Johnson MB, Krsnik Z, Mayer S, Fertuzinhos S, Umlauf S, Lisgo SN, Vortmeyer A, Weinberger DR, Mane S, Hyde TM, Huttner A, Reimers M, Kleinman JE, Sestan N. Spatio-temporal transcriptome of the human brain. *Nature* 2011;478:483–9.
22 Matilla-Duenas A, Ashizawa T, Brice A, Magri S, McFarland KN, Pandolfo M, Pulst SM, Riess O, Rubinsztein DC, Schmidt J, Schmidt T, Scoles DR, Stevanin G, Taroni F, Underwood BR, Sanchez I. Consensus paper: pathological mechanisms underlying neurodegeneration in spinocerebellar ataxias. *Cerebellum* 2014;13:269–302.
23 Harris C, Maroney AC, Johnson EM Jr. Identification of JNK-dependent and -independent components of cerebellar granule neuron apoptosis. *J Neurochem* 2002;83:992–1001.
24 Mei Y, Yuan Z, Song B, Li D, Ma C, Hu C, Ching YP, Li M. Activating transcription factor 3 up-regulated by c-Jun NH(2)-terminal kinase/c-Jun contributes to apoptosis induced by potassium deprivation in cerebellar granule neurons. *Neuroscience* 2008;151:771–9.
25 Dhanasekaran DN, Reddy EP. JNK signaling in apoptosis. *Oncogene* 2008;27:6245–51.
26 Watson A, Eilers A, Lallemand D, Kyriakis J, Rubin LL, Ham J. Phosphorylation of c-Jun is necessary for apoptosis induced by survival signal withdrawal in cerebellar granule neurons. *J Neurosci* 1998;18:751–62.
27 Luo J, Sun Y, Lin H, Qian Y, Li Z, Leonard SS, Huang C, Shi X. Activation of JNK by vanadate induces a Fas-associated death domain (FADD)-dependent death of cerebellar granule progenitors in vitro. *J Biol Chem* 2003;278:4542–51.
28 Kobayashi H, Michiue T, Yukita A, Danno H, Sakurai K, Fukui A, Kikuchi A, Asashima M. Novel Daple-like protein positively regulates both the Wnt/beta-catenin pathway and the Wnt/JNK pathway in Xenopus. *Mech Dev* 2005;122:1138–53.
29 Punta M, Coggill PC, Eberhardt RY, Mistry J, Tate J, Boursnell C, Pang N, Forslund K, Ceric G, Clements J, Heger A, Holm L, Sonnhammer EL, Eddy SR, Bateman A, Finn RD. The Pfam protein families database. *Nucleic Acids Res* 2012;40(Database issue):D290–301.
30 Baron Gaillard CL, Pallesi-Pocachard E, Massey-Harroche D, Richard F, Arsanto JP, Chauvin JP, Lecine P, Kramer H, Borg JP, Le Bivic A. Hook2 is involved in the morphogenesis of the primary cilium. *Mol Biol Cell* 2011;22:4549–62.
31 Rittie L, Fisher GJ. Isolation and culture of skin fibroblasts. *Methods Mol Med* 2005;117:83–98.

Supplemental Methods and Data

A novel missense mutation in *CCDC88C* activates the JNK pathway and causes a dominant form of spinocerebellar ataxia

Ho TSOI, Allen C.S. YU, Zhefan S. CHEN, Nelson K.N. NG, Anne Y.Y. CHAN, Liz Y.P. YUEN, Jill M. ABRIGO, Suk-Ying TSANG, Stephen K.W. TSUI, Tony M.F. TONG, Ivan F.M. LO, Stephen T.S. LAM, Vincent C.T. MOK, Lawrence K.S. WONG, Kwok-Fai LAU, Jacky C.K. NGO, Ting-Fung CHAN and H.Y. Edwin CHAN

Supplemental Methods

Steps in filtering and prioritizing variants

A union set of 328,328 raw variants was identified among the six individuals using GATK UnifiedGenotyper 2.5. The raw variants contain a significant portion of off-target calls, which are outside of the 62 Mb targeted regions as defined by Illumina Truseq Exome Enrichment kit [1]. Sequences outside of the targeted enrichment regions have very low sequencing coverage, therefore the variants within off-target regions were filtered out due to poor quality.

77,841 variants remained upon removing the off-target variant calls. We then proceed to perform variant quality filtering according to the version 4 of GATK best practice for variant detection [2], finally obtaining 70,047 filtered variants. Snpeff [3] was used to annotate the genes (Ensembl GRCh37 release 75) affected by the variants, as well as their predicted functional impact and minor allele frequency in population genetics databases. Following linkage analysis, 615 variants were identified within the regions that showed linkage (see below).

Among the 615 variants in linked regions, 34 of them matched the observed autosomal dominant inheritance pattern (Figure 1A). The Illumina Truseq Exome Enrichment kit does cover 88.3% of exons, promoters, UTRs, microRNAs, and other noncoding RNAs as recorded in RefSeq. We revisited the variant calls and found no evidence of any non-common variants (MAF < 0.005) within the promoter, UTRs, microRNAs, or other noncoding RNAs that fits the observed co-segregation pattern.

Accordingly, synonymous mutations and noncoding mutations were discarded while missense,

splice site mutations, and insertions/deletions were kept, obtaining 13 variants for further analysis. To further exclude common variants, which are unlikely to be causative, we excluded variants with a minor allele frequency greater than 0.005 according to online databases including dbSNP (version 138) [4], 1000 Genomes Project (phase I release version 3) [5], HapMap release 28 [6], and NHLBI Exome Sequencing Project (ESP6500SI-V2) [7]. Variants labelled as pathogenic in these databases were not removed. Only three heterozygous candidate variants remained after this filtering step (Table S4).

Workflow of linkage analysis

Linkdatagen [8] was used to select SNP markers from the 70,047 filtered variants for genetic linkage analysis. Default parameters of Linkdatagen were used, except for changing the population to "Han Chinese in Beijing" from HapMap phase 2. The tool returned 7,443 markers with an average heterozygosity of 0.45 and a frequency of 1 per 0.3 cM, followed by genetic linkage analysis using MERLIN [9]. The genetic map coordinates (cM) was converted to hg18 genome coordinates by linear interpolation of HapMap phase 2 genetic map, followed by lifting over to hg19 genome coordinates by using UCSC liftOver tool. Four linkage regions with log of odds (LOD) score > 2 were identified and they are chr11: 70342417-78811197, chr14:87749314-92755402, chr18:67083133-74211893, and chr20:1189334-2796007.

Supplemental Data

Table S1. Sequencing statistics of the whole-exome sequencing data

	II:1	II:3	II:4	II:5	II:7	II:8
Total reads (in millions)	87.48	59.07	55.92	65.13	62.80	53.74
Total bases (Gbp)	8.84	5.97	5.65	5.64	6.34	5.43
Total post-filtered reads (in millions)	82.36	51.32	48.50	56.06	54.19	46.39
Total post-filtered bases (Gbp)	8.30	5.17	4.89	5.65	5.46	4.67

Statistics of sequencing data from Axeq Technologies before and after reads filtering are listed. To improve accuracy of genotyping, adapter sequences, low quality terminal bases, ambiguous bases, and un-paired singletons were removed from raw sequencing data, using fastq-mcf [10].

Table S2. Quality metrics for exome variant identification of the 6 samples

	II:1	II:3	II:4	II:5	II:7	II:8
Pre-filtering count	275,651	267,977	261,247	265,231	257,778	256,405
Pre-filtering union count	328,328					
Pre-filtering on target count	77,841					
Post-filtering count	70,047					
ts/tv	2.49					
snps/indels	7.52					
Singletons	7,986					
% variants in dbSNP 138 or 1000 Genome DB (phase I release version 3)	96.81					

Abbreviations: ts/tv: Transition/Transversion ratio, which is an indicator of variant filtration effectiveness. N/S: Nonsynonymous / Synonymous variants ratio. Singletons: Found in single sample only. Variant filtering was based on version 4 of the Genome Analysis Toolkit best practice for variant detection.

Table S3. Post-filtering variant prioritization steps

Filters	Number of variants
Located within linked regions (LOD ≥ 2)	615
Conformed to dominant inheritance pattern	34
Missense mutations, splice site mutations, or insertions/ deletions	13
A. Not a common variant	3
B. Predicted to be pathogenic	1
C. Expression patterns	1
D. PubMed search	1
A ∩ B ∩ C ∩ D	1

A—Minor Allele Frequency > 0.005 in dbSNP (version 138), 1000 Genomes Project (phase I release version 3), HapMap release 28, or NHLBI Exome Sequencing Project (ESP6500SI-V2)

B—All functional predictors (SIFT [11], Mutationassessor [12], MutationTaster [13], Polyphen-2 [14] and PROVEAN [15]) predicted the variant as probably damaging or damaging

C—Transcripts Per Million (TPM) > 0 in the brain EST profile of NCBI UniGene.

D—PubMed search of neurologically related citations.

A ∩ B ∩ C ∩ D—Intersection of filter condition A, B, C and D

Table S4. Candidate mutations of SCA40

Location	Ref	Obs	Gene	Mutation	Mutation Assessor	Mutation Taster	Polyphen2 (HumVar)	PROVEAN	SIFT	ABA	HBT	UniGene
chr11: 74413901	C	T	*CHRDL2*	NM_015424: c.G1058A:p.R353H	N (1.590)	N (0.692519)	D (0.910)	N (-1.371)	D (0.030)	1.80	5.96	0
chr14: 90651043	G	A	*KCNK13*	NM_022054: c.G923A:p.R308Q	N (0.895)	N (0.999994)	N (0.006)	N (-1.303)	N (0.146)	2.06	5.25	0
chr14: 91787600	C	T	*CCDC88C*	NM_001080414: c.G1391A:p.R464H	P (2.885)	D (1.0)	P (0.557)	D (-3.813)	D (0.001)	3.30	6.24	2

Abbreviations: Ref—Reference allele, Obs—Observed Allele, ABA—Allen Brain Atlas, HBT—Human Brain Transcriptome, UniGene—brain EST profile of the NCBI UniGene build 236 database.

Functional impact scores were classified as N—Neutral, P—Probably disease causing or D—Disease causing according to the documentation of individual tools. For MutationAssessor [12], PROVEAN [15] and SIFT [11], numbers in the brackets denotes the prediction scores. For MutationTaster [13] and Polyphen 2 [14], numbers in the brackets denotes the confidence of prediction, where a higher value denotes a higher confidence. For Allen Brain Atlas (ABA) and Human Brain Transcriptome (HBT), the average $\log_2$ signal intensities across all samples in cerebellum were shown. For NCBI UniGene, the normalized Transcripts Per Million (TPM) value from the brain EST profile is shown.

Figure S1. Results of parametric genetic linkage analysis

Heterozygous SNPs found in both whole-exome sequencing samples and HapMap phase 2 Chinese Han population were selected such that linkage equilibrium was attained at the frequency of 1 SNP per 0.3 cM. MERLIN was used for multipoint parametric linkage analysis, where a rare dominant disease model with disease allele frequency of 0.00001 was specified.

Figure S2. Overexpression of wildtype (WT) and mutant (MT) forms of CCDC88C, CHRDL2 and KCNK13 proteins in HEK293 cells. Myc-tagged wild type (WT) and mutant (MT) *CCDC88C* (GenBank accession number: NM_001080414), *CHRDL2* (GenBank accession number: NM_015424.4) and *KCNK13* (GenBank accession number: NM_022054) cDNA sequences were synthesized from GenScript USA Inc., and then subcloned into *pcDNA3.1* expression vector. All three sets of WT and MT expression constructs (1 µg) were independently used to transfect HEK293 cells. Cells were harvested 24 hours after transfection and the expression of the myc-tagged proteins were detected by anti-myc antibody 71D10 (1:1,000; Cell Signaling Technology). Anti-JNK 3708 (1:1,000, Cell Signaling Technology) and anti-p-JNK 5136 (1:1,000; Cell Signaling Technology) antibodies were used to detect endogenous JNK. Tubulin was used as loading control and was detected using anti-beta tubulin antibody E7 (1:10,000; Developmental Studies Hybridoma Bank). The experiment was repeated for at least three times. Only representative blots are shown.

Figure S3. Wildtype (WT) and mutant (MT) forms of *CCDC88C* induced dose-dependent phosphorylation of JNK in HEK293 cells. To overexpress CCDC88C protein in HEK293 cells, different amount (0.2 – 1.0 µg) of the *pcDNA3.1* WT and MT *CCDC88C* expression constructs

were used independently to transfect HEK293 cells. "-" denotes untransfected control. Cells were harvested 24 hours after transfection and expression of the CCDC88C proteins were detected by anti-myc antibody 71D10 (1:1,000; Cell Signaling Technology). Anti-JNK 3708 (1:1,000, Cell Signaling Technology) and anti-p-JNK 5136 (1:1,000; Cell Signaling Technology) antibodies were used to detect the total and phosphorylated form of endogenous JNK respectively. Tubulin was used as loading control and was detected using anti-beta tubulin antibody E7 (1:10,000; Developmental Studies Hybridoma Bank). The experiment was repeated for at least three times. Only representative blots are shown.

Figure S4. Overexpression of wildtype (WT) and mutant (MT) forms of *CCDC88C*, and knockdown of endogenous *CCDC88C* expression in HEK293 cells. (A) Overexpression of CCDC88C proteins in HEK293 cells. Both WT and MT *CCDC88C* expression constructs (0.5 µg) were used to transfect HEK293 cells. Cells were harvested 24 hours after transfection and expression of the CCDC88C proteins were detected by anti-myc antibody 71D10 (1:1,000; Cell Signaling Technology). (B) Small interfering RNA (siRNA) treatment reduced endogenous CCDC88C protein expression. HEK293 cells were treated with 5 pmol of ON-TARGETplus *CCDC88C* siRNA L-033364-00-0005 (Dharmacon) or control (ctrl) siRNA (Dharmacon). Protein expression of endogenous CCDC88C was detected by anti-CCDC88C antibody A302-951A (1:1,000; Bethyl Laboratories). Tubulin was used as loading control in all experiments and was detected using anti-beta tubulin antibody E7 (1:10,000; Developmental Studies Hybridoma Bank). The experiment was repeated for at least three times. Only representative blots are shown.

Figure S5. Domain organization of CCDC88C and the location of the p.R464H mutation.

CCDC88C consists of a N-terminal HOOK domain, a central coiled-coil region, a C-terminal disorder region, and a PDZ-binding motif (Gly-Cys-Val). The R464H missense mutation is located within the HOOK domain region. Domain information of the protein was fetched from Pfam [16] and Uniprot [17].

Figure S6. Subcellular localization of wildtype (WT) and mutant (MT) forms of CCDC88C proteins. HEK293 cells were transfected with 1 µg of WT or MT *CCDC88C* expression construct. Cells were harvested 24 hours after transfection and subcellular localization of the CCDC88C proteins was determined using an Olympus FV-1000IX81-TIRF confocal microscope. Primary antibody used was rabbit anti-myc antibody 71D10 (1:500; Cell Signaling Technology) and secondary antibody used was FITC-conjugated goat anti-rabbit antibody (1:500; Zymed). Nuclei were stained with Hoechst 33342 (1:400; Life Technologies). Scale bar represents 5 µm. The experiment was repeated for at least three times. Only representative images are shown.

Supplemental References:

1. Illumina. TruSeq Exome Enrichment Kit Support-Downloads. Secondary TruSeq Exome Enrichment Kit Support-Downloads 2013. http://support.illumina.com/sequencing/sequencing_kits/truseq_exome_enrichment_kit/downloads.ilmn.
2. DePristo MA, Banks E, Poplin R, Garimella KV, Maguire JR, Hartl C, Philippakis AA, del Angel G, Rivas MA, Hanna M, McKenna A, Fennell TJ, Kernytsky AM, Sivachenko AY, Cibulskis K, Gabriel SB, Altshuler D, Daly MJ. A framework for variation discovery and genotyping using next-generation DNA sequencing data. Nat Genet 2011;**43**(5):491-8.
3. Cingolani P, Platts A, Wang le L, Coon M, Nguyen T, Wang L, Land SJ, Lu X, Ruden DM. A program for annotating and predicting the effects of single nucleotide polymorphisms, SnpEff: SNPs in the genome of Drosophila melanogaster strain w1118; iso-2; iso-3. Fly (Austin) 2012;**6**(2):80-92.
4. Sherry ST, Ward MH, Kholodov M, Baker J, Phan L, Smigielski EM, Sirotkin K. dbSNP: the NCBI database of genetic variation. Nucleic Acids Res 2001;**29**(1):308-11.
5. Genomes Project C, Abecasis GR, Altshuler D, Auton A, Brooks LD, Durbin RM, Gibbs RA, Hurles ME, McVean GA. A map of human genome variation from population-scale sequencing. Nature 2010;**467**(7319):1061-73.
6. International HapMap C, Altshuler DM, Gibbs RA, Peltonen L, Altshuler DM, Gibbs RA, Peltonen L, Dermitzakis E, Schaffner SF, Yu F, Peltonen L, Dermitzakis E, Bonnen PE, Altshuler DM, Gibbs RA, de Bakker PI, Deloukas P, Gabriel SB, Gwilliam R, Hunt S, Inouye M, Jia X, Palotie A, Parkin M, Whittaker P, Yu F, Chang K, Hawes A, Lewis LR, Ren Y, Wheeler D, Gibbs RA, Muzny DM, Barnes C, Darvishi K, Hurles M, Korn JM, Kristiansson K, Lee C, McCarrol SA, Nemesh J, Dermitzakis E, Keinan A, Montgomery SB, Pollack S, Price AL, Soranzo N, Bonnen PE, Gibbs RA, Gonzaga-Jauregui C, Keinan A, Price AL, Yu F, Anttila V, Brodeur W, Daly MJ, Leslie S, McVean G, Moutsianas L, Nguyen H, Schaffner SF, Zhang Q, Ghori MJ, McGinnis R, McLaren W, Pollack S, Price AL, Schaffner SF, Takeuchi F, Grossman SR, Shlyakhter I, Hostetter EB, Sabeti PC, Adebamowo CA, Foster MW, Gordon DR, Licinio J, Manca MC, Marshall PA, Matsuda I, Ngare D, Wang VO, Reddy D, Rotimi CN, Royal CD, Sharp RR, Zeng C, Brooks LD, McEwen JE. Integrating common and rare genetic variation in diverse human populations. Nature 2010;**467**(7311):52-8.
7. Tennessen JA, Bigham AW, O'Connor TD, Fu W, Kenny EE, Gravel S, McGee S, Do R, Liu X, Jun G, Kang HM, Jordan D, Leal SM, Gabriel S, Rieder MJ, Abecasis G, Altshuler D, Nickerson DA, Boerwinkle E, Sunyaev S, Bustamante CD, Bamshad MJ, Akey JM, Broad GO, Seattle GO, Project NES. Evolution and functional impact of rare coding variation from deep sequencing of human exomes. Science 2012;**337**(6090):64-9.
8. Smith KR, Bromhead CJ, Hildebrand MS, Shearer AE, Lockhart PJ, Najmabadi H, Leventer RJ, McGillivray G, Amor DJ, Smith RJ, Bahlo M. Reducing the exome search space for mendelian diseases using genetic linkage analysis of exome genotypes. Genome Biol 2011;**12**(9):R85.
9. Abecasis GR, Cherny SS, Cookson WO, Cardon LR. Merlin--rapid analysis of dense genetic maps using sparse gene flow trees. Nat Genet 2002;**30**(1):97-101.
10. Aronesty E. ea-utils : "Command-line tools for processing biological sequencing data". Secondary ea-utils : "Command-line tools for processing biological sequencing data"

2011. http://code.google.com/p/ea-utils.
11. Ng PC, Henikoff S. SIFT: Predicting amino acid changes that affect protein function. Nucleic Acids Res 2003;**31**(13):3812-4.
12. Reva B, Antipin Y, Sander C. Predicting the functional impact of protein mutations: application to cancer genomics. Nucleic Acids Res 2011;**39**(17):e118.
13. Schwarz JM, Rodelsperger C, Schuelke M, Seelow D. MutationTaster evaluates disease-causing potential of sequence alterations. Nat Methods 2010;**7**(8):575-6.
14. Adzhubei I, Jordan DM, Sunyaev SR. Predicting functional effect of human missense mutations using PolyPhen-2. Curr Protoc Hum Genet 2013;**Chapter 7**:Unit7 20.
15. Choi Y, Sims GE, Murphy S, Miller JR, Chan AP. Predicting the functional effect of amino acid substitutions and indels. PLoS One 2012;**7**(10):e46688.
16. Punta M, Coggill PC, Eberhardt RY, Mistry J, Tate J, Boursnell C, Pang N, Forslund K, Ceric G, Clements J, Heger A, Holm L, Sonnhammer EL, Eddy SR, Bateman A, Finn RD. The Pfam protein families database. Nucleic Acids Res 2012;**40**(Database issue):D290-301.
17. UniProt C. Activities at the Universal Protein Resource (UniProt). Nucleic Acids Res 2014;**42**(Database issue):D191-8.

Figure S1

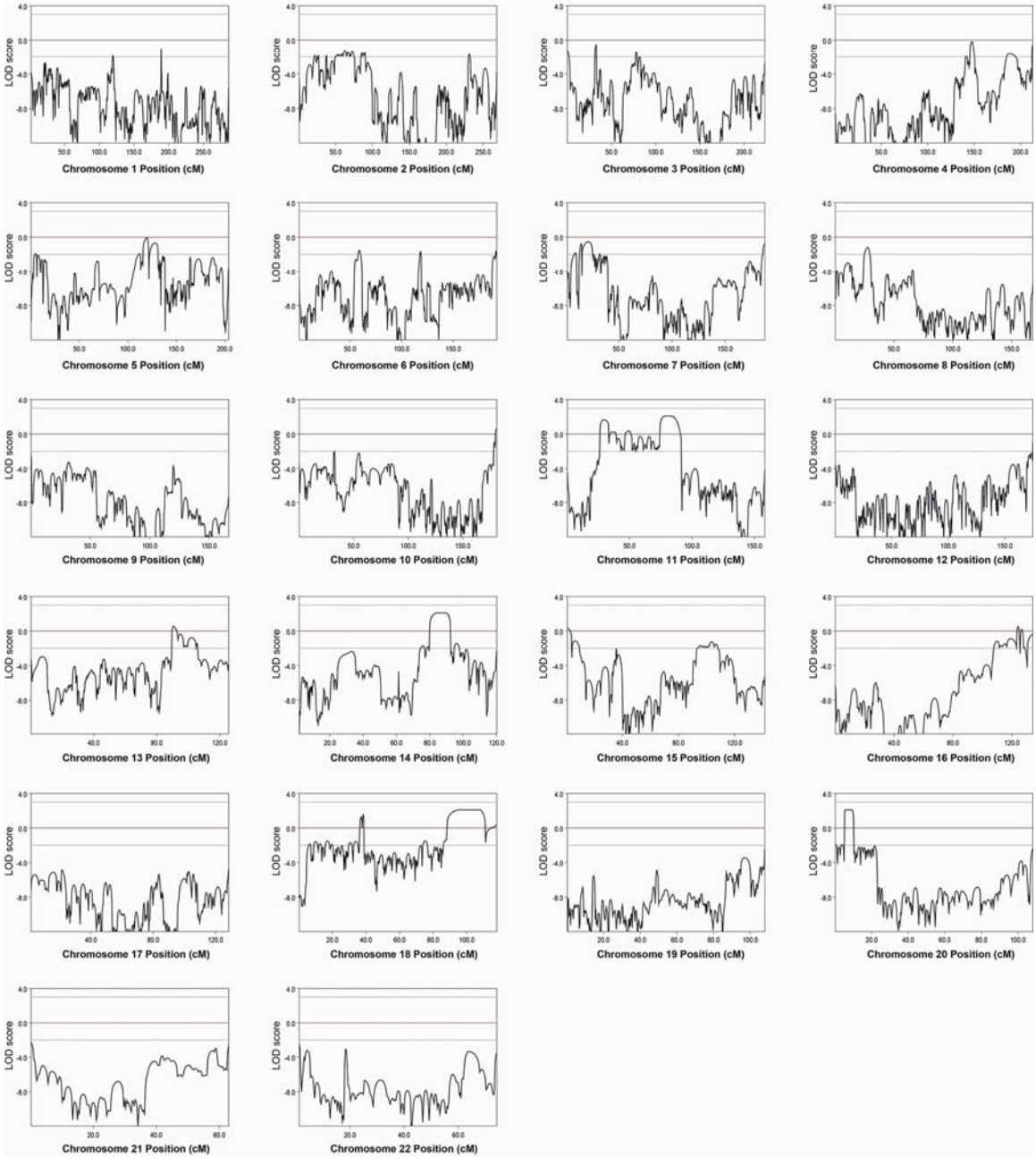
LOD score
Chromosome 1 Position (cM)
Chromosome 2 Position (cM)
Chromosome 3 Position (cM)
Chromosome 4 Position (cM)
Chromosome 5 Position (cM)
Chromosome 6 Position (cM)
Chromosome 7 Position (cM)
Chromosome 8 Position (cM)
Chromosome 9 Position (cM)
Chromosome 10 Position (cM)
Chromosome 11 Position (cM)
Chromosome 12 Position (cM)
Chromosome 13 Position (cM)
Chromosome 14 Position (cM)
Chromosome 15 Position (cM)
Chromosome 16 Position (cM)
Chromosome 17 Position (cM)
Chromosome 18 Position (cM)
Chromosome 19 Position (cM)
Chromosome 20 Position (cM)
Chromosome 21 Position (cM)
Chromosome 22 Position (cM)

Figure S2

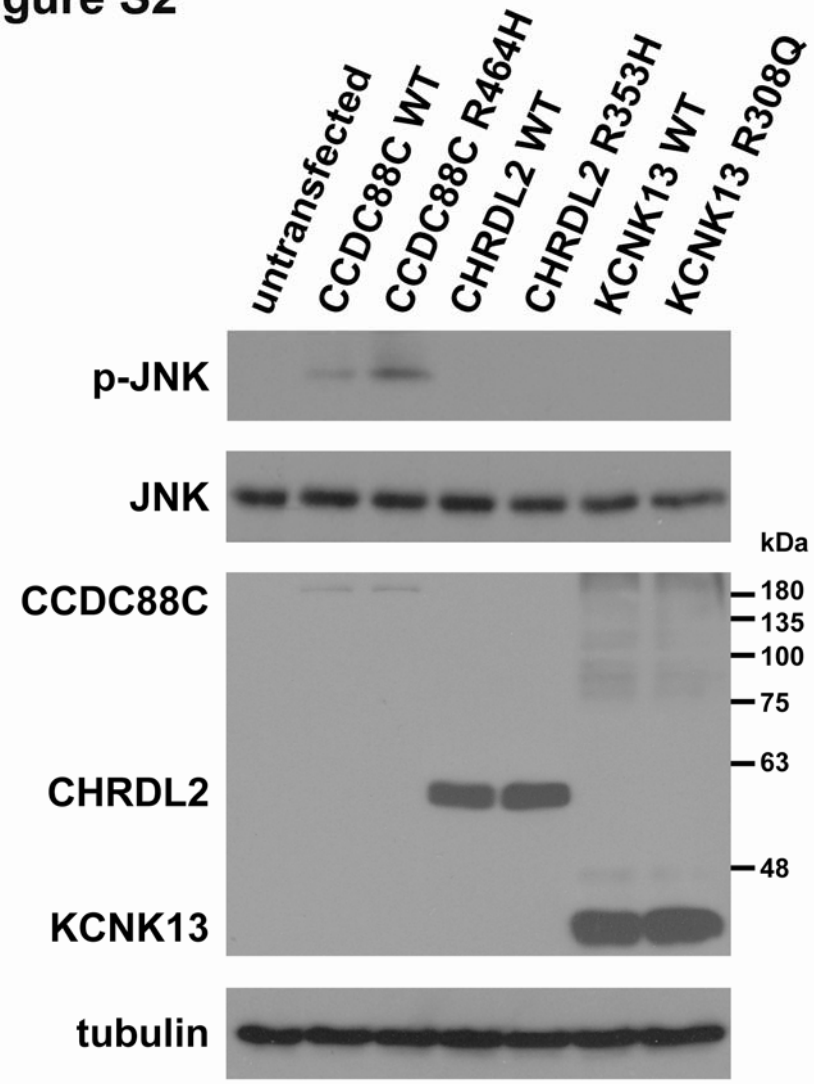
untransfected
CCDC88C WT
CCDC88C R464H
CHRDL2 WT
CHRDL2 R353H
KCNK13 WT
KCNK13 R308Q
p-JNK
JNK
kDa
CCDC88C
180
135
100
75
63
CHRDL2
48
KCNK13
tubulin

Figure S3

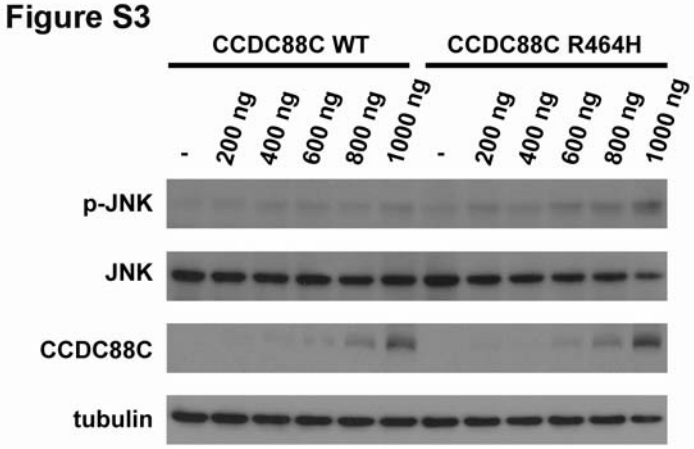
CCDC88C WT
CCDC88C R464H
-
200 ng
400 ng
600 ng
800 ng
1000 ng
-
200 ng
400 ng
600 ng
800 ng
1000 ng
p-JNK
JNK
CCDC88C
tubulin

Figure S4

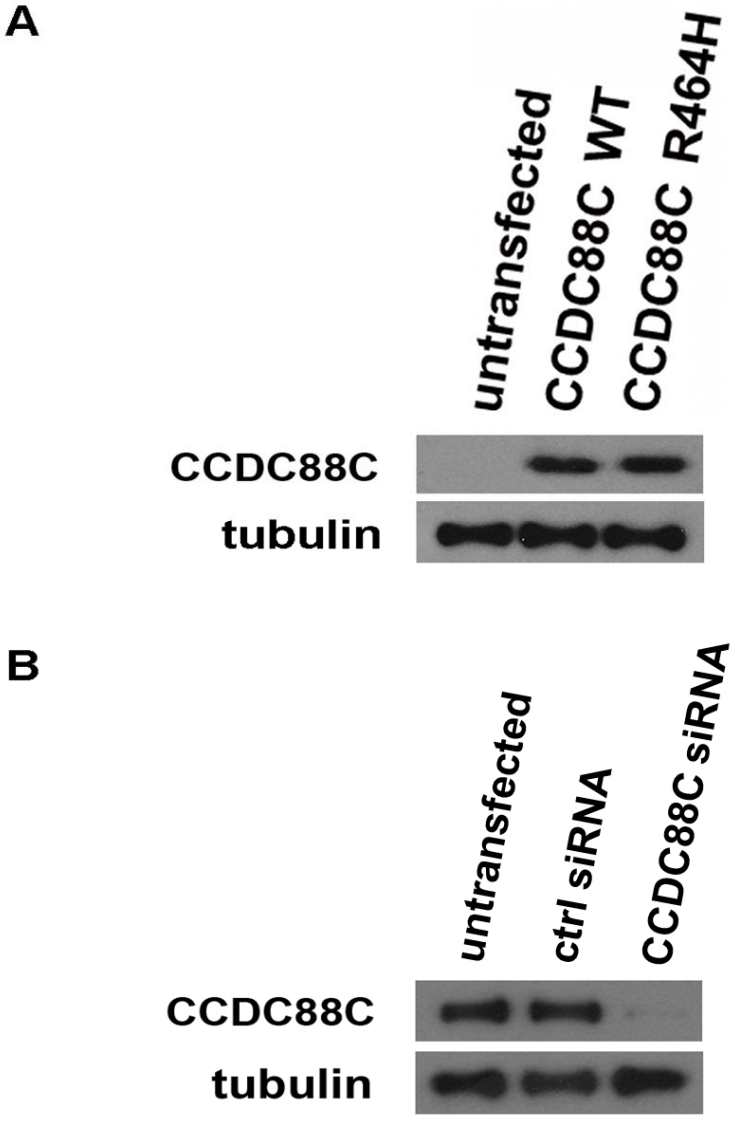
A
untransfected
CCDC88C WT
CCDC88C R464H
CCDC88C
tubulin
B
untransfected
ctrl siRNA
CCDC88C siRNA
CCDC88C
tubulin

Figure S5

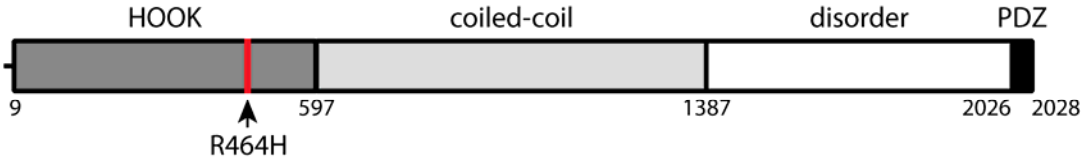

Figure S6